JOURNAL OF APPLIED POLYMER SCIENCE VOL. 19, 3277–3290 (1975)

Studies on Blown Film Extrusion. II. Analysis of the Deformation and Heat Transfer Processes

CHANG DAE HAN and JONG YOO PARK, *Department of Chemical Engineering, Polytechnic Institute of New York, Brooklyn, New York 11201*

Synopsis

Having investigated the elongational flow behavior of polymer melts (part I of this series), we have carried out both theoretical and experimental studies in order to better understand the deformation and heat transfer processes involved in blown film extrusion. For the experimental study, nonisothermal experiments were carried out, using high-density and low-density polyethylenes. Measurements were taken of the axial tension, bubble diameter, and film thickness at a series of extrusion conditions (i.e., flow rate, pressure difference across the film, and take-up speed). For the theoretical study, an analysis was carried out to simulate the blown-film extrusion process, by setting up the force- and energy-balance equations on the blown bubble moving upward. The approach taken in the theoretical study may be considered as an extension of the earlier work by Pearson and Petrie who considered the isothermal operation of Newtonian fluids. In the present study, however, we have considered the nonisothermal operation of power law fluids, whose rheological parameters were determined by an independent experimental study as described in part I of this series. Four highly nonlinear differential equations were solved numerically with the aid of the CDC 360 digital computer, using the fourth-order Runge-Kutta method. The mathematical model predicts the bubble shape, temperature profile, and film thickness as a function of the distance along the machine axis. Comparison is made of the experimentally observed bubble shapes with the theoretically predicted ones, showing a reasonable agreement.

INTRODUCTION

The blown film process may be considered as combining features of blow molding and flat film extrusion. An advantage of the blown film process over the flat film process lies in that the former permits one to have biaxially oriented film, whereas the latter produces uniaxially oriented film. Since the degree of orientation of macromolecules governs the physical properties of the finished film, such as the tensile strength, tear resistance, and heat seal characteristics, it is expected that the biaxially oriented film would have better physical properties than the uniaxially oriented film would.

As in fiber spinning, in the blown film process there are two important processing variables which affect the orientation of macromolecules. These are the rate of stretching and the rate of cooling. It should be noted that both the rate of cooling and the rate of stretching affect the degree of crystallinity in crystalline polymers. In the blown film process, however, there is an additional processing variable which can significantly affect the orientation of molecules, namely, the air pressure inside the inflated bubble (i.e., the pressure difference across the thin film).

Only a few theoretical studies of the blown film process are reported in the literature. Pearson[1] appears to be the first who attempted to analyze the blown film process from a fluid-mechanical point of view. More recently, Pearson and Petrie[2,3] and Petrie[4] have discussed the problem theoretically in some depth. However, these authors dealt *only* with the isothermal operation of Newtonian fluids[2,3] and of an Oldroyd type of viscoelastic fluid.[4]

From the practical processing point of view, the analysis of Pearson and Petrie[2,3] has two shortcomings. One is that the industrial operation is practiced under nonisothermal conditions. As pointed out above, the rate of cooling is one of the most important processing variables and can significantly affect the quality of the finished product. Another is that the thermoplastics (e.g., polyethylene) being used for making blown films are non-Newtonian fluids at processing conditions. Our study, reported in part I of the series,[5] indeed shows the non-Newtonian behavior of film forming polymers in the blown film process.

The purpose of this paper, the second of this series, is to present our recent study on the development of a mathematical model simulating the nonisothermal blown film processing of power law fluids and to compare the theoretical prediction with our experimental results.

EXPERIMENTAL

In the present study, we carried out nonisothermal blown-film extrusion experiments, using high-density polyethylene (HDPE) and low-density polyethylene (LDPE). These are the same materials used in our previous work on isothermal blown film extrusion.[5]

The apparatus and experimental procedure employed in the present study were the same as that described in part I of this series,[5] except that the film was extruded into the ambient (i.e., the isothermal chamber was removed). In the experiment, the shape of the bubble was photographed under each extrusion condition, and the tension was measured using a Tensitron tensiometer at a position just below the nip rolls. Samples were collected and the film thickness was measured along the machine direction.

The purpose of the experimental work was to provide information for checking the validity of the theoretical work described below.

THEORETICAL DEVELOPMENT

The approach taken here is very similar to that of Pearson and Petrie,[2,3] insofar as the force balance equation is concerned. However, the present study has three distinct features which distinguish it from theirs. First, the energy balance is included in the system differential equations so that the nonisothermal operation of the blown film process can be simulated. Second, instead of the Newtonian fluid model considered by Pearson and Petrie,[2,3] a power law model based on a separate experimental study (part I of this series) is employed, taking into account the temperature dependence of the material constants involved. Third, the effect of gravity is included in the force balance equation. It should be noted that, in the upward extrusion which is a feature of the blown film process, the inclusion of the gravity effect

in the force balance equation is very important because the film's weight is supported by regions of increasing melt strength. Note further that the force exerted on the film by the take-up device should counterbalance the gravity force which acts in the direction opposite to the machine direction.

We make the following assumptions in the derivation of the force and energy balance equations: (1) the film is thin enough so that variations in the flow field across it may be neglected; (2) the velocity gradients may be approximated locally by those of a plane film being extended biaxially; (3) the effects of surface tension, air drag, and inertial force are negligible compared to the axial tension (i.e., the rheological force needed for the deformation of the bubble of molten polymer); (4) the heat transfer between the inner surface and the air trapped within the bubble is negligible; (5) the heat of crystallization (if the material is crystallizable) is negligible; (6) the heat conduction in the film is negligible; (7) the cooling of the bubble is controlled by radiative and convective heat transfer; (8) the heat generation due to the frictional force is negligible.

Force Balance Equation

The force balance equations are given as[5]

$$2\pi a \cos\theta P_L + \pi\Delta p(A^2 - a^2) + 2\pi\rho g \int_z^Z ah \sec\theta dz = F_Z \tag{1}$$

$$\Delta p = \frac{P_L}{R_L} + \frac{P_H}{R_H} - \rho g h \sin\theta \tag{2}$$

where

$$F_Z = F_L - 2\pi\rho_s g A H(L - Z) \tag{3}$$

$$P_L = hT_{11} \tag{4}$$

$$P_H = hT_{33} \tag{5}$$

$$R_H = a/\cos\theta \tag{6}$$

$$R_L = -\sec^3\theta \Big/ \frac{d^2a}{dz^2} \tag{7}$$

In order to extend the usefulness of these force balance equations into the nonisothermal blown film process, we propose the following semiempirical expression for the material function:

$$\eta_B(\Pi, T) = \eta_0 e^{E/R\left(\frac{1}{T} - \frac{1}{T_0}\right)}[\Pi/2]^{\frac{n-1}{2}} \tag{8}$$

in which E is the activation energy in elongational flow, R is the gas constant, η_0 is the elongational viscosity at reference temperature T_0, T is the film temperature, Π is the second invariant of the rate-of-strain tensor [see eq. (24) of ref. 5], and n is a material constant. This expression is based on the experimental study described in part I of this series.[5]

Since T_{11} in eq. (4) can be expressed in terms of η_B and components of the rate-of-strain tensor [see eqs. (27) and (28) of ref. 5], we have

$$P_L = -\frac{2\eta_B(\Pi, T)Q\cos\theta}{2\pi a}\left[\frac{1}{a}\frac{da}{dz} + \frac{2}{h}\frac{dh}{dz}\right] \tag{9}$$

$$P_H = \frac{2\eta_B(\Pi, T)Q\cos\theta}{2\pi a}\left[\frac{1}{a}\frac{da}{dz} - \frac{1}{h}\frac{dh}{dz}\right]. \tag{10}$$

Now, defining the dimensionless variables

$$r = a/a_0,\ w = h/a_0,\ x = z/a_0,\ s = T/T_0 \tag{11}$$

in which a_0 is the radius of a bubble at $z = 0$ and T_0 is the melt temperature at $z = 0$ (i.e., at the die exit), eqs. (1) and (2) may be rewritten, with the aid of eqs. (6), (7), (9), and (10), as follows:

$$\frac{w'}{w} = -\frac{r'}{2r} - \frac{\eta_0[T_g + r^2B]\sec^2\theta}{4\eta_B(\Pi, s)} \tag{12}$$

$$2r^2[T_g + r^2B]r'' = \frac{6r'\eta_B(\Pi, s)}{\eta_0} + r\sec^2\theta[T_g - 3r^2B] \tag{13}$$

where

$$B = \frac{a_0^3\pi\Delta p}{Q\eta_0} \tag{14}$$

$$T_g = \frac{a_0}{Q\eta_0}\left[F_Z - 2\pi\rho g a_0^3\int_x^X rw\sec\theta\,dx\right] - B[A/a_0]^2 \tag{15}$$

$$X = Z/a_0. \tag{16}$$

Using the geometrical relationship (see Fig. 4 of ref. 5), we have

$$\frac{da}{dz} = \tan\theta \tag{17}$$

which may be rewritten in terms of the dimensionless variable r:

$$r' = \tan\theta \tag{18}$$

which then gives

$$r'' = \sec^2\theta\,\theta'. \tag{19}$$

Substituting eqs. (18) and (19) into eq. (13), we obtain

$$2r^2[T_g + r^2B]\theta' = \frac{3\sin 2\theta\,\eta_B(\Pi, s)}{\eta_0} + r[T_g - 3r^2B] \tag{20}$$

in eqs. (12)–(20), w', r', and θ' are the first-order derivatives of w, r, and θ with respect to x, and $\eta_B(\Pi,s)$ may be expressed in terms of dimensionless variables as

$$\eta_B(\Pi, s) = \alpha e^{\beta/s}\left[\frac{Q\cos\theta}{2\pi a_0^3}\right]^{n-1}\left[\frac{1}{rw}\right]^{n-1}\left[\left(\frac{w'}{w}\right) + \left(\frac{r'}{r}\right) + \left(\frac{r'w'}{rw}\right)\right]^{\frac{n-1}{2}} \tag{21}$$

in which α and β are defined as

$$\alpha = \eta_0 e^{-E/RT_0}, \beta = E/RT_0 \tag{22}$$

At this point, it may be worth pointing out that eqs. (12), (18), and (20) reduce to the expressions derived by Pearson and Petrie[3]:

$$\frac{w'}{w} = -\frac{r'}{r} - \frac{[T_F + r^2B]\sec^2\theta}{4} \tag{23}$$

$$r' = \tan\theta \tag{24}$$

$$2r^2[T_F + r^2B]\theta' = 3\sin 2\theta + r[T_F - 3r^2B] \tag{25}$$

where

$$T_F = \frac{a_0F_Z}{Q\eta_0} - B[A/a_0]^2 \tag{26}$$

for isothermal process of a Newtonian liquid [i.e., $T = T_0$ and $n = 1$ in eq. (8)] and when the effect of gravity is neglected.

Energy Balance Equation

Based on the assumptions stated above, an energy balance on the film may be written as follows:

$$\rho C_v v_1 \frac{\partial T}{\partial \xi_1} = \frac{\partial q}{\partial \xi_2} \tag{27}$$

in which ρ is the fluid density, C_v is the specific heat capacity, v_1 is the velocity in ξ_1 direction (see the coordinate systems given in Fig. 4 of ref. 5), and q is the heat flux in ξ_2 direction. Multiplying both sides of eq. (27) by $d\xi_2$ and integrating the resulting equation from $\xi_2 = 0$ to $\xi_2 = h$ gives

$$\rho C_v \frac{Q\cos\theta}{2\pi a}\frac{dT}{dz} = U(T - T_a) + \lambda\epsilon(T^4 - T_a^4). \tag{28}$$

in which the following boundary conditions were used:
(i) at $\xi_2 = 0$ (inner surface)

$$q = 0 \tag{29}$$

(ii) at $\xi_2 = h$ (outer surface)

$$q = U(T - T_a) + \lambda\epsilon(T^4 - T_a^4). \tag{30}$$

Note that, in eq. (28), we have used the following relationship:

$$\frac{\partial T}{\partial \xi_1} = \frac{dT}{dz}\frac{dz}{d\xi_1} = \frac{dT}{dz}\cos\theta \tag{31}$$

$$v_1 = Q/2\pi ah \tag{32}$$

and U is the overall heat transfer coefficient, λ is the Stefan-Boltzmann constant, ϵ is emissivity, T_a is the ambient temperature, and Q is the volumetric flow rate.

Equation (28) may be rewritten as

$$s' = rD \sec \theta (s - s_a) + rE \sec \theta (s^4 - s_a{}^4) \tag{33}$$

in which s is the dimensionless temperature as defined by eq. (11), s' is the derivative of s with respect to x, and D and E are dimensionless parameters as defined by

$$D = (UT_0)\Big/\left(\frac{\rho C_v Q T_0}{2\pi a_0{}^2}\right), \quad E = (T_0{}^4 \lambda \epsilon)\Big/\left(\frac{\rho C_v Q T_0}{2\pi a_0{}^2}\right). \tag{34}$$

Governing System Equations and Computational Procedure

For simulating the nonisothermal blown film process with a non-Newtonian fluid of power law type, one has to solve eqs. (12), (18), (20), and (33), with the aid of eqs. (15) and (21). By differentiating eqs. (12) and (20) with respect to x, with the aid of eq. (15), we can transform the differential-integral equations into higher-order differential equations. However, solution of the resulting equations requires additional boundary conditions which are not known a priori from the physical point of view. This could pose a very difficult problem with the numerical integration of the differential equations.

In order to avoid the anticipated mathematical difficulties in solving the differential-integral equations, we adopted the following computational procedure which treated the problem as solving four first-order differential equations, by a trial-and-error procedure. We first assumed a value for T_g appearing in eqs. (12) and (20), and then numerically integrated eqs. (12), (18), (20), and (33) with the boundary conditions:

(i) at x = 0,

$$r = 1.0, \; w = h_0/a_0, \; s = 1.0, \; \theta = \theta_0 \tag{35}$$

(ii) at $x = X \; (= Z/a_0)$,

$$r = A/a_0, \; w = H/a_0, \; s = T_s/T_o, \; \theta = 0. \tag{36}$$

Then, we checked if eq. (15) was satisfied. If eq (15) was not satisfied, numerical integration of eqs. (12), (18), (20), and (33) was repeated with new guesses of T_g until it was satisfied. This computational procedure was found very effective in the actual simulation study.

RESULTS AND DISCUSSION

Having presented a mathematical model for the simulation of the blown film process, we shall now discuss some representative results of model prediction, namely, how the shape of a bubble, the profile of film thickness, and the temperature profile of a bubble vary with variations in processing conditions, namely, the pressure difference ΔP and the stretch ratio V_L/V_0. We will then make a comparison of the theoretically predicted with experimentally observed bubble shapes and film thicknesses.

Model Predictions

Figure 1 gives the predicted shape, and Figure 2, the temperature profile, of a bubble, for different values of stretch ratio V_L/V_0. Note that, because of symmetricity, only one half of the bubble is shown in Figure 1. It is seen that the bubble shape and temperature profiles are relatively insensitive to variations in stretch ratio.

Figures 3 and 4 show the effects of pressure difference on bubble shape and temperature profile, respectively. It is seen that both the shape and temperature profile are very sensitive to variations in B [see eq. (14) for the definition of B]. A close look at Figure 3 shows that the bubble with larger values of B (i.e., greater pressure difference) has a less inflated shape than the one with lower values of B, which may seem to be contradictory to our intuitive expectation. However, as Pearson and Petrie[3] correctly pointed out, this can

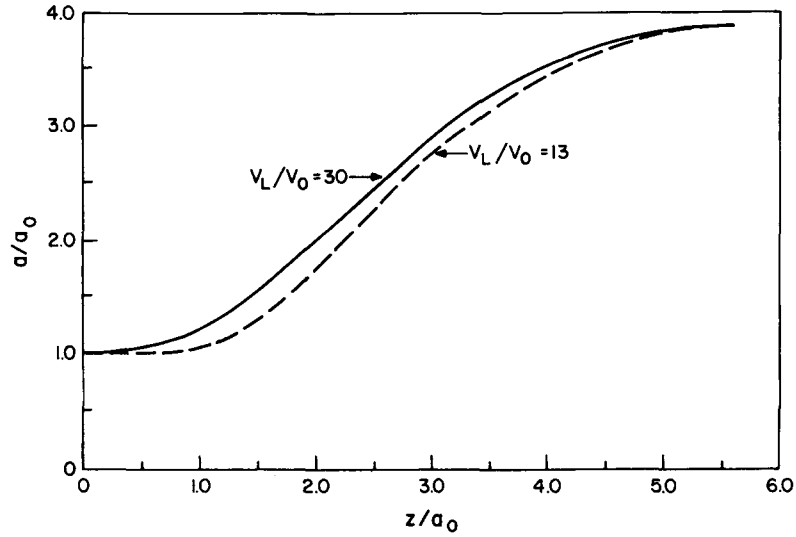

Fig. 1. Effect of stretch ratio V_L/V_0 on the shape of a bubble. System parameters: n = 0.796, β = 7.448, B = 0.384, D = 0.00865, E = 0.01014.

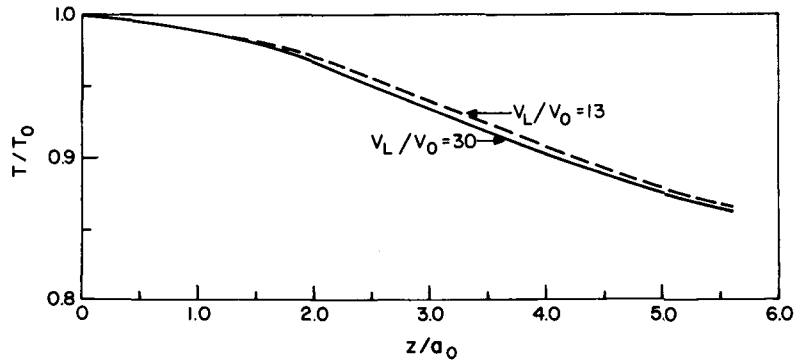

Fig. 2. Effect of stretch ratio V_L/V_0 on the temperature profile of a bubble. System parameters same as in Fig. 1.

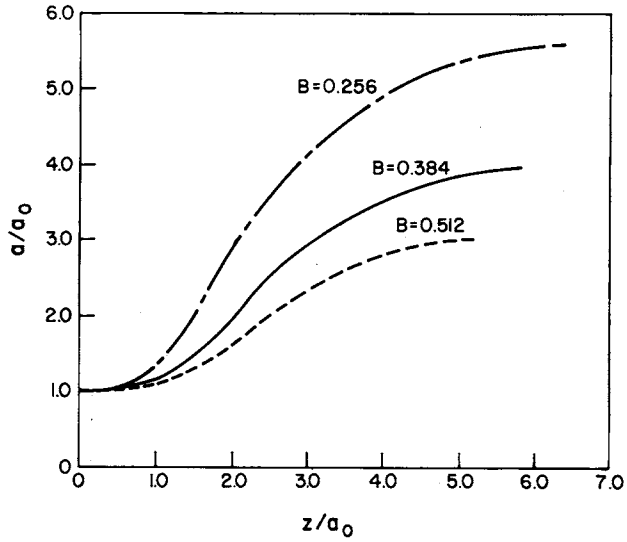

Fig. 3. Effect of pressure difference B on the shape of a bubble. System parameters: n = 0.796, β = 7.448, V_L/V_0 = 30, D = 0.00865, E = 0.01014.

be understood when one considers the fact that, in order to balance the surface tension forces between the inflated bubble and the air, a greater excess pressure (i.e., ΔP) will be required for a smaller bubble radius (i.e. consider $\Delta P = \sigma/a$, in which σ is the surface tension and a is the radius of a bubble). It should be kept in mind that we are concerned here with steady-state conditions for different values of pressure difference, and not with the transient response of the bubble to a pressure change.

Under identical cooling conditions, we expect that the temperature of a larger bubble (i.e., a thinner film) will be lower than that of a smaller bubble (i.e., a thicker film). This indeed is predicted from the simulation, as given in Figure 4.

Two of the parameters involved in the material function, defined by eq. (8), can affect the shape of a bubble. They are n and η_0, and they may be considered to be characteristic of a material. Figure 5 gives the shape of a bubble

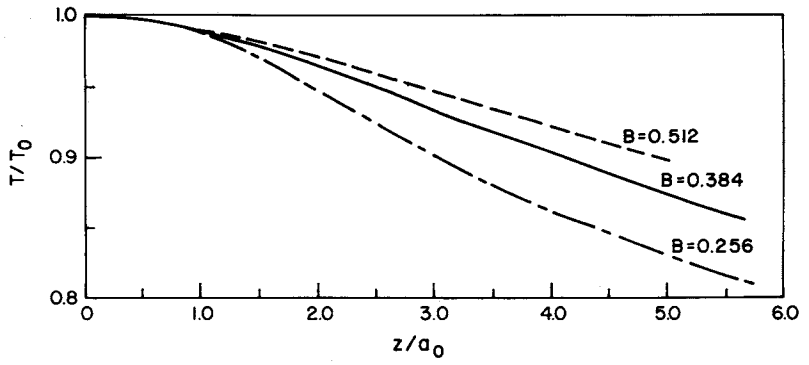

Fig. 4. Effect of pressure difference B on the temperature profile of a bubble. System parameters same as in Fig. 3.

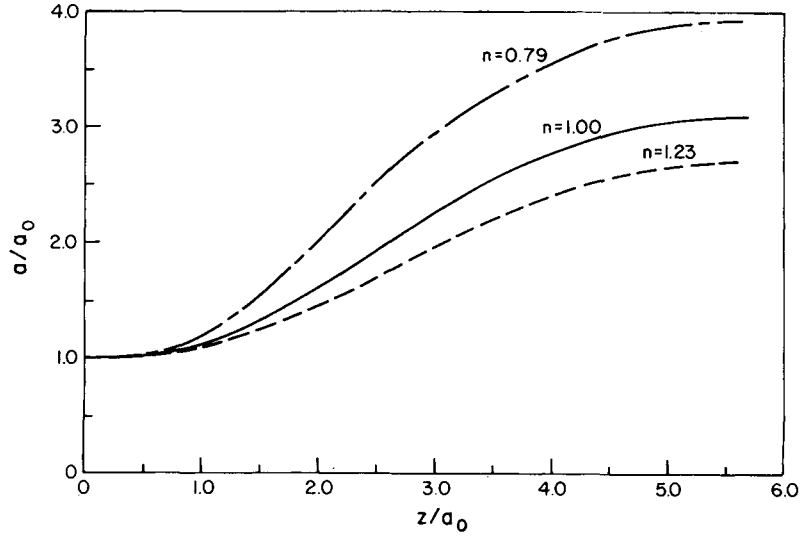

Fig. 5. Effect of the material constant n on the shape of a bubble. System parameters: $V_L/V_0 = 30, \beta = 7.448, B = 0.384, D = 0.00865, E = 0.01014$.

for different values of n. It should be remembered[5] that there are some materials whose elongational viscosities increase with elongation rate (i.e., $n > 1$) and others whose elongational viscosities decrease with elongation rate (i.e., $n < 1$). It is interesting to note in Figure 5 that the material with $n < 1$ gives rise to a larger bubble than the one with $n > 1$. Figure 6 gives the temperature profiles of bubbles for materials with different values of n. That the material with $n < 1$ gives rise to lower bubble temperature than the one with $n > 1$ is as expected, in view of the relationship existing between the bubble size and bubble temperature, as mentioned above in reference to Figures 3 and 4.

With the definition of B given in eq. (14), one can also make use of Figures 3 and 4 for discussing the effect of η_0 on the bubble shape and bubble temperature. Since η_0 is the elongational viscosity at reference temperature T_0, one may conclude from Figure 3 that materials having lower elongational viscosi-

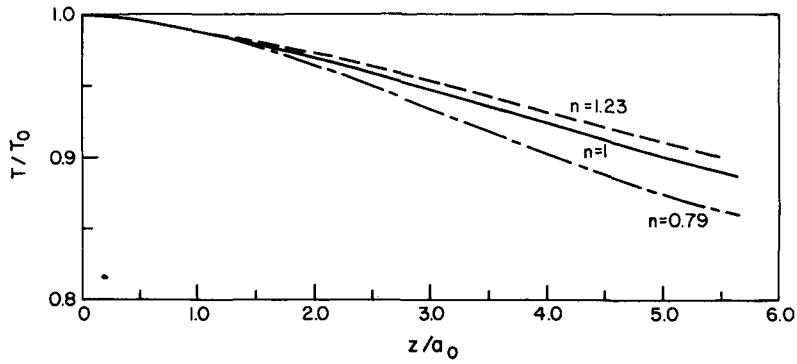

Fig. 6. Effect of the material constant n on the temperature profile of a bubble. System parameters same as in Fig. 5.

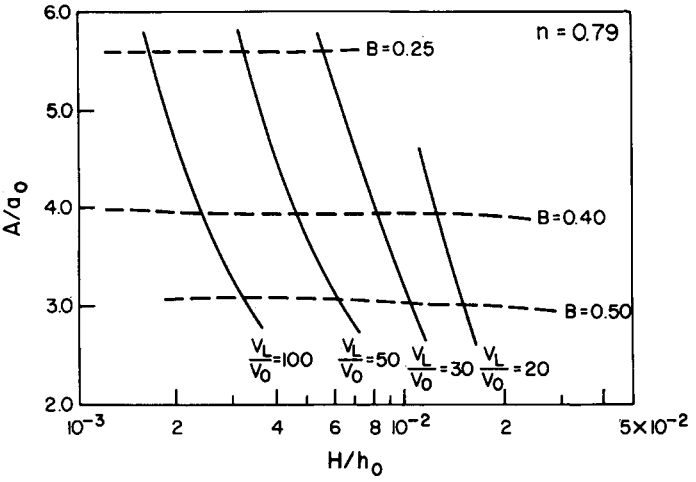

Fig. 7. Blow-up ratio vs. film thickness reduction for the material having $n = 0.79$. System parameters: $\beta = 7.448, D = 0.00865, E = 0.01014$.

ties (i.e., large values of B) give rise to bubbles smaller than those of materials having higher elongational viscosities (i.e., small values of B).

For the purpose of running the blown film process, one would be interested in having a sort of operating guide which would give the relationship between the blow-up ratio A/a_0 and the thickness reduction H/h_0 at different processing conditions. Note that A and H are the bubble radius and film thickness, respectively, at and above the frost line, assuming that the change in film thickness above the frost line is negligibly small. To illustrate the point, two representative results are given in Figure 7 for $n = 0.79$ and in Figure 8 for $n = 1.23$.

The reason why the take-up ratio V_L/V_0 instead of the tension F_L was used for presenting the results given above is because, in a commercial plant, one rarely measures the tension of a bubble, but one can always measure the

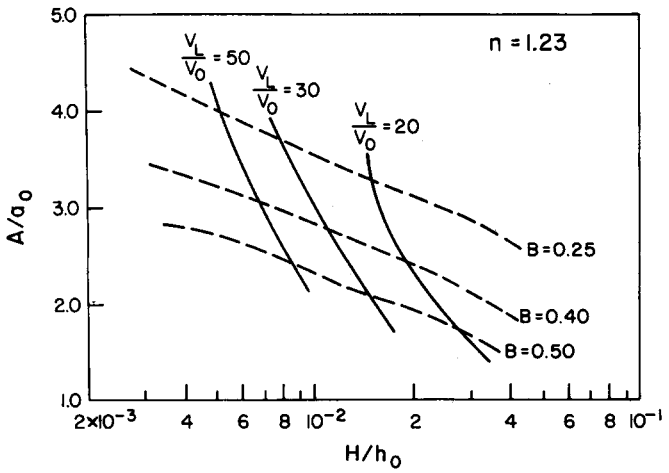

Fig. 8. Blow-up ratio vs. film thickness reduction for the material having $n = 1.28$. System parameters same as in Fig. 7.

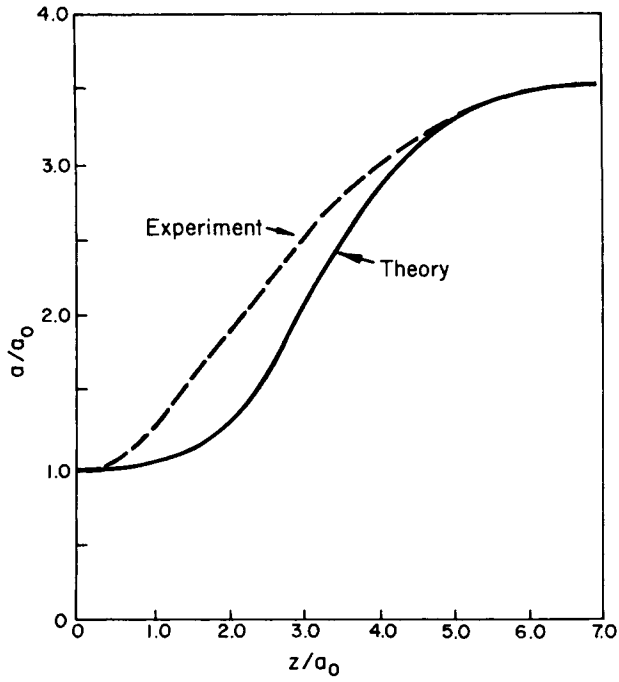

Fig. 9. Comparison of the experimentally observed bubble shape with the theoretically predicted one for high-density polyethylene. Extrusion conditions: $T = 200°C$, $Q = 20.93$ g/min, $n = 0.79$, $V_0 = 0.346$ cm/sec, $V_L/V_0 = 17.5$, $\Delta p = 1.87 \times 10^{-2}$ psi.

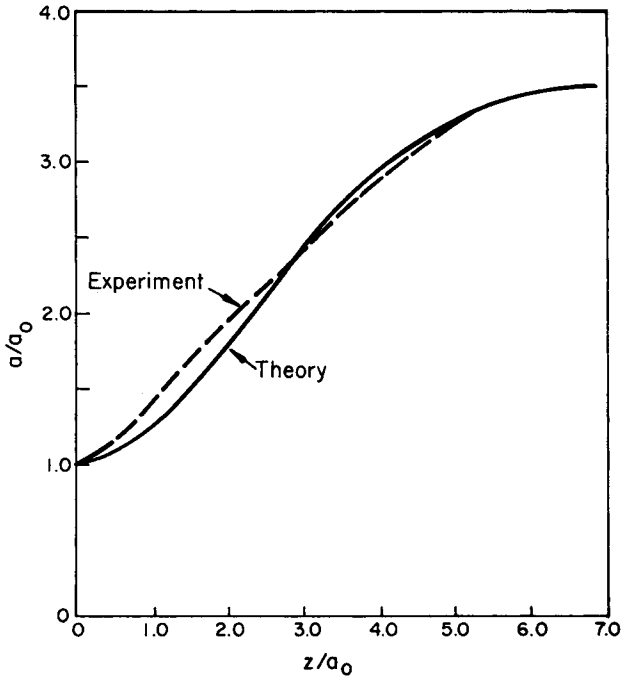

Fig. 10. Comparison of the experimentally observed bubble shape with the theoretically predicted one for low-density polyethylene. Extrusion conditions: $T = 200°C$, $Q = 18.10$ g/min, $n = 1.28$, $V_0 = 0.377$ cm/sec, $V_L/V_0 = 12.4$, $\Delta p = 0.79 \times 10^{-2}$ psi.

speed of the take-up roller. However, in our experiment, both tension and take-up speed were measured.

It is of interest to note that the theoretically predicted temperature profiles are of very similar shape to experimentally observed ones.[6–8]

A Comparison of the Predicted and Experimental Results

Figures 9 and 10 give representative results of experimentally observed bubble shapes of high-density polyethylene and low-density polyethylene, respectively. Figures 11 and 12 give experimentally determined profiles of the film thickness for the same polymers. Table I gives a summary of the numerical values of the physical parameters for the high-density and low-density polyethylenes used. It can be said that agreement between the experimentally observed and the theoretically predicted bubble shapes is reasonable, in view of the fact that a number of assumptions were made in the derivation of the force and energy balance equations, and that there is some uncertainty over the numerical values of several physical parameters (e.g., C_v, h, λ, ϵ). Note that the numerical values of α, β, E, and n are estimated ones by using the experimentally obtained elongational viscosity data reported in part I of this series.[5] Note, also, that because of the lack of experimental data we have neglected the temperature dependence of density ρ in the region between the die exit and the frost line (i.e., $0 \leq z < Z$). However, consideration of the temperature dependence of density will not affect the theoretical prediction much. This is because as a molten blown film is solidified, its density may vary as much as 30% at most, whereas its viscosity will vary by at least one order of magnitude.

Certain parameters were assumed for computational purposes, and therefore might have affected the theoretical prediction because of the lack of experimental data. One such parameter is the position of the frost line ($z = Z$). Theoretically speaking, the frost line is the position at which deformation of a film ceases, i.e., the film thickness remains constant for $z \geq Z$. In practice, however, there can still be a reduction in film thickness at positions beyond the frost line. For instance, it is well known that low-density polyethylene can be stretched even at room temperature, when the film is very thin. In the present study, bubble temperature was not measured, and consequently the frost line was determined based on the visual observation of the blown bubble moving upward. We could have obtained a better estimate of the position of the frost line if we had measured temperature profiles in the direction of bubble travel.

TABLE I
Summary of the Numerical Values of the Physical Parameters Used in Simulation

Material	Reference temp., °C	α	β	E, cal/mole	n	ρ, g/cc
High-density polyethylene	200	2.07×10^3	5.13	4.83×10^3	0.79	0.761
Low-density polyethylene	200	6.88×10^3	4.06	3.82×10^3	1.28	0.718

Another uncertain parameter involved in analyzing the data is the initial thickness of a film, i.e., $h = h_0$ at $z = 0$. Extrudate swell is observed in blown film extrusion (as it is in capillary extrusion). Hence, the true initial thick-

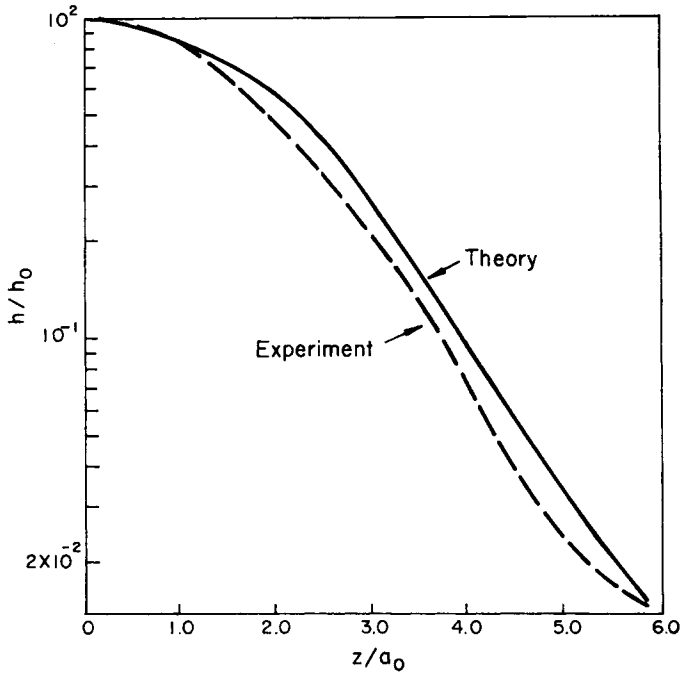

Fig. 11. Comparison of the experimentally determined film thickness with the theoretically predicted one for high-density polyethylene. Extrusion conditions same as in Fig. 9.

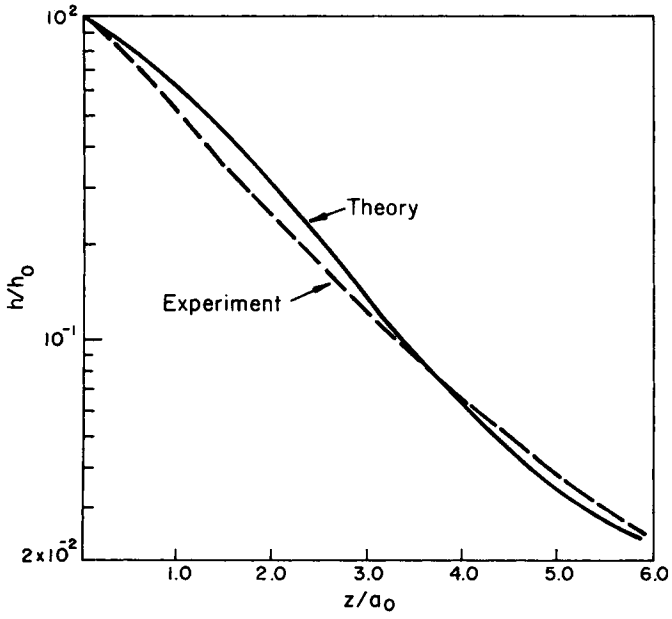

Fig. 12. Comparison of the experimentally determined film thickness with the theoretically predicted one for low-density polyethylene. Extrusion conditions same as in Fig. 10.

ness of a film must have been greater than that used in actual computation, i.e., the distance between the inner and outer cylinder, which in the present case is $h_0 = 0.030$ in. In practice, however, it was virtually impossible to obtain the true value of h_0 experimentally.

CONCLUSIONS

A mathematical model for simulating the blown film process has been developed, taking into account the heat transfer between the molten film and the coolant, and the effect of gravity. Also, a power law type of empirical expression for describing the rheological property pertinent to the blown film process has been used, relating the elongational viscosity to the second invariant of the rate-of-strain tensor in biaxial stretching. The model has been tested against experimentally observed profiles of bubble diameter and film thickness of low-density and high-density polyethylene films. It has been found that there is a discrepancy between the theoretically predicted and experimentally observed profiles, although agreement between the two may seem reasonable. Explanations are offered for the observed discrepancy between the theoretically predicted and experimentally observed results.

This work is taken in part from the dissertation of J. Y. Park, submitted to the Faculty of the Polytechnic Institute of New York in partial fulfillment of the requirements for the degree of Doctor of Philosophy, 1975.

References

1. J. R. A. Pearson *Mechanical Principles of Polymer Melt Processing,* Pergamon Press, London, 1966.
2. J. R. A. Pearson and C. J. S. Petrie, *J. Fluid Mech.*, **40**, 1 (1970); *ibid.*, **42**, 609 (1970).
3. J. R. A. Pearson and C. J. S. Petrie, *Plast. Polym.*, **38**, 85 (1970).
4. C. J. S. Petrie, *Rheol. Acta,* **12**, 92 (1973).
5. C. D. Han and J. Y. Park, *J. Appl. Polym. Sci.*, **19**, 3257 (1975).
6. L. E. Dowd, *SPE J.* **28**, 22 (1972).
7. R. Farber, M. S. Thesis (Ch.E.), McGill University, Montreal, Canada, 1973.
8. R. Farber and J. Dealy, *Polym. Eng. Sci.*, **14**, 435 (1974).

Received November 5, 1974
Revised April 21, 1975